NOTES AND CORRESPONDENCE

On the Joint Role of Subtropical Atmospheric Variability and Equatorial Subsurface Heat Content Anomalies in Initiating the Onset of ENSO Events

Bruce T. Anderson

Department of Geography, Boston University, Boston, Massachusetts

(Manuscript received 19 January 2006, in final form 10 August 2006)

ABSTRACT

Previous research has shown that seasonal mean variations in both the subtropical/extratropical sea level pressures over the central North Pacific and the subsurface heat content anomalies in the western equatorial Pacific are significantly related to the state of the El Niño–Southern Oscillation (ENSO) 12–18 months later. Here we find that positive (negative) subsurface temperature anomalies in the western equatorial Pacific during boreal summer/fall, followed by negative (positive) anomalies in the sea level pressure fields over the subtropical central North Pacific during boreal winter, tend to result in positive (negative) mature ENSO events 12–15 months later (i.e., during the following boreal winter). When the intervening sea level pressure anomalies are of the same sign as the preceding heat-content anomalies, the correlation between the heat-content anomalies and the following boreal-winter ENSO state disappears. There is still some relation between the boreal-winter sea level pressure anomalies and the ENSO state the following year when the two precursor patterns are of the same sign; however, the correlation is smaller and the ENSO events tend to be weaker. Additional analysis indicates that the two precursor fields are related to one another; however, the sea level pressure variations contain more unique information about, and provide better predictability of, the state of the following ENSO system than do the heat content anomalies.

1. Introduction

The El Niño–Southern Oscillation (ENSO) phenomenon is a coupled mode of variability of the ocean–atmosphere system in the equatorial Pacific characterized by a relative warming/cooling of the sea surface temperatures (SSTs) over the eastern equatorial Pacific and a change in the zonal sea level pressure gradient across the basin (Philander 1985). While the time scale for this oscillation is typically considered to be 3–6 yr, it has been found that there is a boreal-spring "predictability barrier" preventing the use of equatorial Pacific SSTs themselves to predict mature ENSO events (which typically occur during boreal winter; Larkin and Harrison 2002) at time scales longer than approximately 9 months (Torrence and Webster 1998). However, theoretical and observational results suggest that preceding temperature anomalies in the *subsurface* equatorial Pacific can be present up to a year before mature ENSO events (Jin 1997; Li 1997; Meinen and McPhaden 2000, 2001; McPhaden 2003) and that these anomalies can initiate the onset of overlying SST anomalies following the boreal spring "predictability barrier" (McPhaden 2003). In addition, precursor fields in the subtropical/extratropical atmospheric fields also appear to overcome this "predictability barrier" and are related to the initiation of ENSO events that develop over the course of the following 9–12 months (Kidson 1975; Trenberth 1976; Reiter 1978; Rasmusson and Carpenter 1982; van Loon and Shea 1985, 1987; Barnett 1985; Trenberth and Shea 1987; Lysne et al. 1997; Gu and Philander 1997; Li 1997; Barnett et al. 1999; Pierce et al. 2000; Wang 2001; Vimont et al. 2001, 2003; Anderson 2003, 2004).

Here we will examine the joint relation of the seasonal-mean tropical/extratropical atmosphere structure and tropical Pacific heat content anomalies to the onset of boreal-winter ENSO events. In section 2, the various datasets used in this study are described. The relation between tropical Pacific sea surface temperature anomalies and antecedent atmospheric and oceanic variability is examined in section 3. Findings are summarized and briefly discussed in section 4.

Corresponding author address: Bruce T. Anderson, Department of Geography, Boston University, 675 Commonwealth Ave., Boston, MA 02215-1401.
E-mail: brucea@bu.edu

DOI: 10.1175/JCLI4075.1

2. Data

The principal atmospheric dataset used in this investigation is the reanalysis product from the National Centers for Environmental Prediction (NCEP; see acknowledgments). Details about this dataset, including its physics, dynamics, and numerical and computational methods, are discussed in Kalnay et al. (1996) and Kistler et al. (2001). For this paper, we focus on the monthly mean sea level pressures because they contain significant precursor information regarding the development of large-scale SST anomalies in the equatorial Pacific (Kidson 1975; Trenberth 1976; van Loon 1984; van Loon and Shea 1985, 1987; Barnett 1985; Trenberth and Shea 1987; B. Wang et al. 1999; Chan and Xu 2000; Wang 2001; Larkin and Harrison 2002; Vimont et al. 2003; Anderson 2003). These fields are represented at 2.5° resolution in both the meridional and zonal direction, encompassing a total of 144 × 73 grid points. We choose to use the reanalysis product owing to its fairly long continuous record (1948–2003 here) and its systematic treatment of observational and numerical data over this entire period.

In addition to the reanalyzed atmospheric fields, this study will also examine the time evolution of the seasonal-mean subsurface ocean state. For this field we archive the observational analysis from the Joint Environmental Data Analysis Center (JEDAC), which uses an optimal interpolation procedure to produce 5° × 2.5° gridded values of temperature, mixed layer depth, and heat content [vertically integrated from the surface to 400 m (White 1995; W. B. White 2003, personal communication)] at monthly time scales from 1955 to 2003. Here we focus on the heat content anomalies (also referred to as heat storage anomalies) because these have also been shown to be significantly related to the onset and development of large-scale SST anomalies in the equatorial Pacific (e.g., McPhaden 2003). While estimates of tropical oceanic heat content anomalies prior to about 1980 are generally reduced compared with the period following the 1980s (Chepurin and Carton 1999), we find that results using a subset of data during this latter time period are qualitatively (and quantitatively) the same as those derived from the full time series. Here we use the full time series in order to increase the robustness of the results.

To capture variability in the equatorial Pacific sea surface temperature field, we archive the Niño-3.4 index provided by the National Oceanic and Atmospheric Administration's (NOAA) Climate Diagnostics Center (CDC; see acknowledgments for data availability). This index is defined as the area-average SST anomalies between 5°N–5°S and 170°–120°W. The version used here is derived from the reanalyzed SST fields described in Hurrell and Trenberth (1999).

Throughout this paper, results will be based upon statistical relationships between anomalous values of various fields. For the heat content fields (Fig. 2) we tested the significance of these results explicitly by performing a bootstrap analysis following the methodology of Ebisuzaki (1997). This method retains the autocorrelation structure of the gridpoint and index time series, as well as their possible non-Gaussian distributions. In addition, it retains any spatially correlated features the gridpoint fields might have. We find that except in very localized regions, correlation values of $|r| = 0.35$ are above the 95% confidence interval (not shown), which we set as the confidence interval for this figure.

3. Results

Previous research has shown that there exists a precursor mode of boreal-winter sea level pressure (SLP) variability in the central tropical/extratropical North Pacific that precedes variations in the January–March ENSO by approximately 12–15 months (Barnett 1985; Trenberth and Shea 1987; Chan and Xu 2000; Vimont et al. 2003; Anderson 2003). This mode of SLP variability can be captured by a sea level pressure index (SLPI) centered on 10°–25°N and 140°–175°W (Anderson 2003). The SLPI is constructed by calculating the monthly gridpoint sea level pressure anomalies with respect to the climatological value for the given month and then normalizing these gridpoint anomalies by their interannual standard deviation. The normalized monthly anomalies are then area averaged over 10°–25°N and 140°–175°W to arrive at monthly values for the SLPI. While the index itself is defined for the tropical central North Pacific region, it is significantly correlated with additional SLP anomalies over the subtropical and extratropical North Pacific (Anderson 2003, 2004) and as such we refer to it as a "subtropical" index in order to differentiate it from the tropically centered SLP anomalies typically associated with the ENSO system.

The seasonal-mean value of the SLPI from November to March is shown in Fig. 1 and indicates a significant negative correlation ($r = -0.61$) with the boreal-winter (January–March) ENSO state 12–15 months later (note that the concurrent correlation between the boreal-winter SLPI and Niño-3.4 index is $r = 0.05$). Previous observational and modeling studies suggest seasonal mean variations in the boreal-winter sea level pressure fields in the SLPI region can influence the initiation and development of the ENSO system by modifying the wind stress fields over the central tropi-

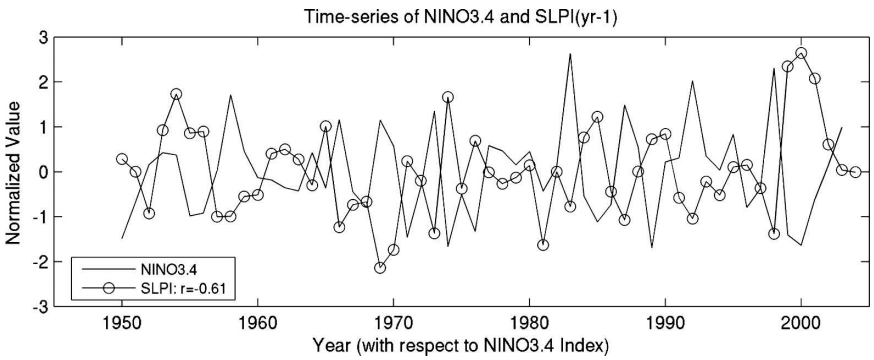

FIG. 1. Time series of boreal-winter (November–March) seasonal mean SLPI anomalies, defined as the area-average gridpoint sea level pressure anomalies over 10°–25°N and 140°–175°W (circles); time series is shifted forward 12 months (i.e., the 1948 value is plotted in 1949). Also shown is the time series of the January–March Niño-3.4 index for the current year (solid line). Both time series normalized by their respective interannual standard deviations.

cal Pacific, which in turn are related to concurrent changes in the underlying subsurface temperature structure of the equatorial/tropical Pacific (Wang et al. 2003; Anderson 2004; Anderson and Maloney 2006). These same subsurface temperature anomalies are conducive to initiating overlying surface temperature anomalies the following spring, which then develop into mature ENSO events by the following boreal winter (Jin 1997; Meinen and McPhaden 2000).

Figure 2 shows the evolution of this subsurface temperature structure, as represented by the 3-month mean heat storage anomalies from 0 to 400 m, regressed against the seasonal-mean November–March SLPI, starting 9 months before the November–March SLPI period and progressing through the period concurrent with the SLPI. Here we multiply the heat storage regression values by -1 in order to present the related heat-storage evolution preceding positive ENSO events (i.e., El Niños). During the preceding boreal summer there are significant equatorial anomalies over the western Pacific indicative of anomalously warm subsurface temperatures in this region (there are no corresponding anomalies in the overlying equatorial SSTs; not shown). During the boreal fall and early boreal winter, these heat content anomalies migrate eastward toward the central Pacific and intensify during the late boreal winter concurrent with the SLPI. However, significant warm-water SST anomalies do not appear in the central and eastern equatorial Pacific until the following May–July period (Anderson 2003).

These results indicate that there exist precursor subsurface temperature signatures prior to periods of anomalous sea level pressures in the SLPI region. In turn, these results suggest that the ability of the SLPI anomalies during a given winter to initiate ENSO events may be dependent upon the existence of such subsurface temperature signatures, similar to what has been found for westerly wind bursts (Moore and Kleeman 1999; Perigaud and Cassou 2000; Fedorov 2002).

To test this hypothesis, we calculated a western Pacific heat storage index (HST index) by area averaging the heat storage anomalies over the region 5°N–5°S and 160°E–180° (the core of the positive correlations seen in Figs. 2d,e). We then calculated the 5-month mean for all 5-month periods preceding the November–March SLPI and selected the period with the highest overall correlation with the SLPI. The selected period, from June to October, has a correlation with the seasonal mean November–March SLPI of $r = -0.49$. Not unexpectedly, the June–October HST index is also significantly correlated with the January–March Niño-3.4 index 18 months later ($r = 0.57$).

However, when the June–October HST index and the following November–March SLPI are conditioned upon whether they have the same or opposite sign (Fig. 3), it is found that the boreal-summer/fall western Pacific HST index is much more strongly correlated with the January–March Niño-3.4 index 18 months later if the HST index has the opposite sign as the intervening SLPI compared with years in which it has the same sign ($r = 0.69$ and $r = 0.06$, respectively). The correlation of the boreal-winter SLPI with the January–March Niño-3.4 index one year later is also higher if the SLPI is preceded by anomalous western equatorial heat content anomalies of the opposite sign ($r = -0.72$) compared with years in which the heat content anomalies are of the same sign ($r = -0.37$). In addition to having a weaker correlation with the preceding SLPI (which is only significant at the 90% level for the 17 events shown here), the strength of the Niño-3.4 index (rep-

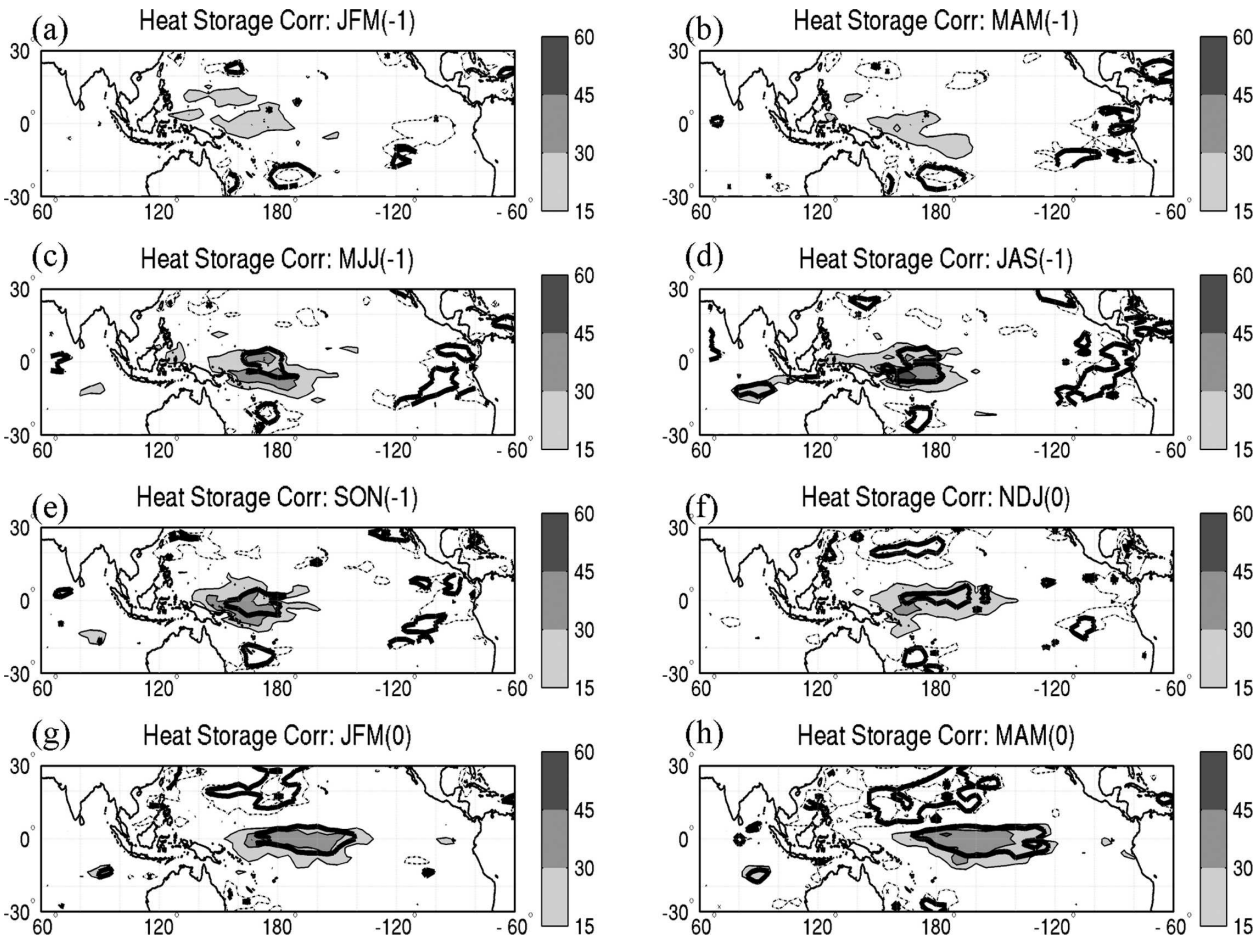

FIG. 2. Three-month mean HST anomalies from 0 to 400 m regressed against the seasonal mean SLPI anomalies for November–March. Initials give the respective three-month period. Numeral indicates lead/lag relation to January period of SLPI (−1: year prior to SLPI; 0: year concurrent with SLPI). All regression values are multiplied by −1 to represent the evolution preceding positive ENSO events. Contour interval is 15×10^7 W s m^{-2}; minimum contour is $\pm 15 \times 10^7$ W s m^{-2}. Thick line represents regions with correlations greater than $|r| = 0.35$ (approximately the 95% confidence limit using bootstrapping methodology; see text). (a) January–March HST preceding the SLPI; (b) March–May HST; (c) May–July HST; (d) July–September HST; (e) September–November HST; (f) November–January HST concurrent with the SLPI; (g) January–March HST; (h) March–May HST.

resented by its interannual variance) is also weaker following years in which the SLPI and western Pacific HST index have the same sign as compared with years in which they have the opposite sign ($\sigma^2_{\text{NINO3.4}} = 0.40$ compared with $\sigma^2_{\text{NINO3.4}} = 1.45$; for the full time series $\sigma^2_{\text{NINO3.4}} = 1.0$ by definition).

To test whether the difference in the opposite-sign and same-sign composite SLPI/Niño-3.4 and HST/Niño-3.4 correlations described above are simply an artifact of the compositing procedure itself, we created and selected 1000 randomly generated 47-yr time series for each index such that they had approximately the same overall correlations as observed [i.e., r(HST/Niño-3.4) = 0.57 ± 0.025, r(SLPI/Niño-3.4) = −0.61 ± 0.025, and r(HST/SLPI) = −0.49 ± 0.025]. For each of the 1000 sets of time series, we performed the same compositing procedure based upon the sign of the artificial SLPI and HST time series and then correlated the composited time series with the composited artificial Niño-3.4 time series. We find that the mean correlation values for the opposite-sign and same-sign composites are nearly identical (the difference between the two is $\Delta r = 0.0019$ and $\Delta r = 0.0064$ for the mean SLPI/Niño-3.4 and HST/Niño-3.4 correlations, respectively). In addition, the differences between the *observed* opposite-sign/same-sign composite correlations are greater than 95% of the differences derived from the artificial time series. Finally, the opposite-sign composite correlations for the observed SLPI/Niño-3.4 and HST/Niño-3.4 time series ($r = -0.72$ and $r = 0.69$, respectively) are greater than 95% of those derived from the artificial time series while the same-sign composite correlation for the ob-

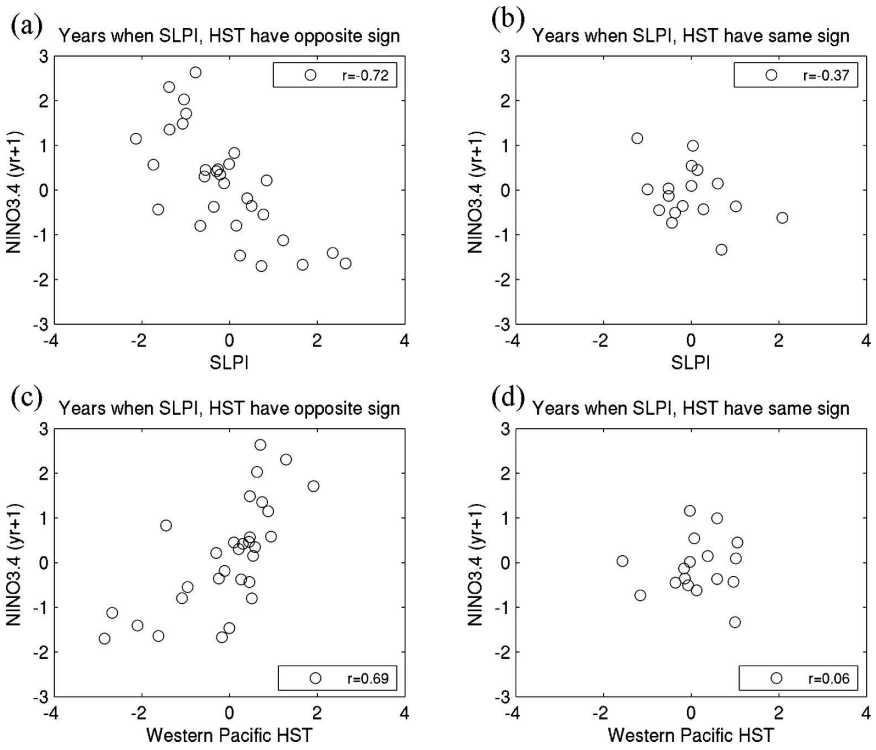

FIG. 3. (a) Scatterplot of the seasonal-mean November–March SLPI with the January–March Niño-3.4 index the following year, plotted only for those years in which the SLPI has the opposite sign as the normalized HST anomalies averaged over the region 5°N–5°S, 160°E–180° during the previous June–October period. (b) Same as in (a), except for only those years in which the SLPI has the same sign as the preceding heat storage anomalies. (c) Scatterplot of the normalized heat storage anomalies averaged over the region 5°N–5°S, 160°E–180°during June–October with the January–March Niño-3.4 index 18 months later, plotted only for those years in which the following November–March SLPI has the opposite sign as heat storage anomalies. (d) Same as in (c), except for only those years in which the SLPI has the same sign as heat storage anomalies.

served HST/Niño-3.4 time series ($r = 0.06$) is less than 95% of those derived from the artificial time series. The same holds for the means, difference of means, and distributions of the composited artificial Niño-3.4 variances. As such we argue that the compositing procedure itself is not likely (at the 95% confidence level) to have spuriously generated the observed opposite-sign/same-sign correlations or variances discussed above.

Overall, it appears that the relation of either the HST index or the SLPI to the development of mature ENSO events is a function of the status of the other index; in addition the two indices are significantly correlated with one another, making it difficult to quantify the relation of the ENSO system to each index separately. One way to do so is to perform a "Granger causality" test (Granger 1969). This test quantifies the difference in predictability provided by the two indices by comparing the residual sum of squares between the actual and predicted values of the January–March Niño-3.4 using two separate estimates. In the first estimate, both the June–October HST index and November–March SLPI, along with the previous year's January–March Niño-3.4 value, are used as optimally weighted linear predictors to estimate the following year's January–March Niño-3.4 value (termed the "unrestricted" prediction). In the second, one of the predictors is removed (the SLPI for instance) and a second estimate is made by optimally weighting the remaining predictors; this estimate is termed the "restricted" prediction. The skill of prediction (in a least squares sense) from the restricted model will always be less than that from the unrestricted model. The difference in the residual sum of squares from the two models quantifies the amount of *nonredundant* variance that is contributed by the predictor that is *removed* from the restricted model. Performing this analysis indicates that 19% of the vari-

ance of the boreal-winter Niño-3.4 is contributed by the SLPI alone. In contrast, only 8% of the variance is uniquely contributed by the western Pacific HST index. Both of these values are significant at the 95% confidence interval with the SLPI-related causality significant at the 99% confidence interval. (Interestingly, the Niño-3.4 index from the previous winter only explains an additional 0.1% of the variance in the following value of the Niño-3.4.)

Similar results are obtained when the predicted time series are generated from out-of-sample forecasts (in which a yearly value from each time series is removed; the linear-statistical model is trained using the remaining values from the time series, and then a forecast is made for the out-of-sample year). In addition, the out-of-sample cross-validation procedure indicates that when both the HST index and SLPI predictors are used, the out-of-sample forecast of the Niño-3.4 index correlates with observed values at $r = 0.69$. When we use only the SLPI as the sole predictor, the correlation drops to $r = 0.64$. However, when we use only the HST index as the sole predictor, the correlation drops further to $r = 0.55$. Overall, these results suggest that the western Pacific HST index does not provide much additional predictability regarding the state of the ENSO system beyond that associated with the SLPI; in addition, they suggest that atmospheric variations in the SLPI region may have a greater influence upon the state of the ENSO system compared with variations in the subsurface heat content anomalies over the western Pacific.

4. Summary

The relationship between interannual variations in the subtropical atmospheric patterns, equatorial Pacific heat content anomalies, and eastern equatorial Pacific SSTs is investigated here. Previous results indicate that the initiation and onset of ENSO events in the tropical Pacific can be partly associated with both seasonal-mean variations in the central subtropical/extratropical Pacific sea level pressure fields as well as in the subsurface heat content anomalies over the western equatorial Pacific. Here we find that years in which there are 1) positive (negative) boreal-summer/fall subsurface temperature anomalies in the western equatorial Pacific and 2) negative (positive) anomalies in the boreal-winter sea level pressure fields over the subtropical central North Pacific tend to result in positive (negative) mature ENSO events during the following boreal winter (i.e., 12–18 months later). When the intervening sea level pressure anomalies are of the same sign as the preceding heat-content anomalies, the correlation of the heat-content anomalies with the following ENSO state disappears; there is still some relation between the boreal-winter sea level pressure anomalies and the ENSO state the following year; however, the correlation is smaller and the ENSO events tend to be weaker under these scenarios.

Here we briefly discuss one possible physical interpretation for these statistical findings. Results presented above suggest that for periods with preexisting subsurface warm-water anomalies in the equatorial western Pacific, there is a much higher probability that these are followed by positive ENSO events if, during the intervening boreal-winter period, there is a *decrease* in the sea level pressure fields over the central subtropical Pacific. This decrease in subtropical sea level pressures in turn is related to a decrease in the trade winds over the tropical North Pacific (Chan and Xu 2000; Anderson 2003, 2004). As described in Li (1997), the curl of these wind stress anomalies over the central Pacific (cf. Figs. 10a, b from Anderson 2003 but reversed) can produce a convergence of meridional Sverdrup transport into the central equatorial Pacific and a subsequent increase in the basin-average thermocline depths. This process can allow for the eastward translation of the western equatorial heat content anomalies into the central and eastern Pacific (Li 1997) as seen in Fig. 2, where they can effectively modify the overlying sea surface temperature fields. Conversely, during years in which there is an *increase* in the sea level pressure fields over the central subtropical Pacific during the intervening boreal winter, the subsequent Sverdrup discharge might limit the eastward translation of the preexisting heat-content anomalies in the western Pacific and hence the initiation of ENSO events. Further diagnosis of these interactions within climate simulation models is currently underway.

It is important to note that we do not argue that the initiation of ENSO events is solely related to variability in the preceding equatorial Pacific heat-content fields and subtropical Pacific sea level pressure fields. A multivariate linear regression of the two indices against the Niño-3.4 index gives a correlation of $|r| = 0.72$, which indicates that only about half of the variance of the ENSO system can be captured by these two indices.

Acknowledgments. Thanks are extended to the reviewers for their insightful and constructive comments. NCEP reanalysis data provided by the NOAA–CIRES Climate Diagnostics Center, Boulder, Colorado, from their Web site at http://www.cdc.noaa.gov. Climate indices provided by NOAA–CIRES Climate Diagnostics Center from their Web site at http://www.cdc.noaa.gov/ClimateIndices/index.html.

REFERENCES

Anderson, B. T., 2003: Tropical Pacific sea surface temperatures and preceding sea level pressure anomalies in the subtropical North Pacific. *J. Geophys. Res.,* **108,** 4732, doi:10.1029/2003JD003805.

——, 2004: Investigation of a large-scale mode of ocean–atmosphere variability and its relation to tropical Pacific sea surface temperature anomalies. *J. Climate,* **17,** 4089–4098.

——, and E. Maloney, 2006: Interannual tropical Pacific sea surface temperatures and their relation to preceding sea level pressures in the NCAR CCSM2. *J. Climate,* **19,** 998–1012.

Barnett, T. P., 1985: Variations in near-global sea level pressure. *J. Atmos. Sci.,* **42,** 478–501.

——, D. W. Pierce, M. Latif, D. Dommenget, and R. Saravanan, 1999: Interdecadal interactions between the tropics and midlatitudes in the Pacific basin. *Geophys. Res. Lett.,* **26,** 615–618.

Chan, J. C. L., and J. Xu, 2000: Physical mechanisms responsible for the transition from a warm to a cold state of the El Niño–Southern Oscillation. *J. Climate,* **13,** 2056–2071.

Chepurin, G. A., and J. A. Carton, 1999: Comparison of retrospective analyses of the global ocean heat content. *Dyn. Atmos. Oceans,* **29,** 119–145.

Ebisuzaki, W., 1997: A method to estimate the statistical significance of a correlation when the data are serially correlated. *J. Climate,* **10,** 2147–2153.

Fedorov, A. V., 2002: The response of the coupled tropical ocean–atmosphere to westerly wind bursts. *Quart. J. Roy. Meteor. Soc.,* **128,** 1–23.

Granger, C. W. J., 1969: Investigating causal relations by econometric models and cross-spectral methods. *Econometrica,* **37,** 424–438.

Gu, D., and S. G. H. Philander, 1997: Interdecadal climate fluctuations that depend on exchanges between the tropics and extratropics. *Science,* **275,** 805–807.

Hurrell, J. W., and K. E. Trenberth, 1999: Global sea surface temperature analyses: Multiple problems and their implications for climate analysis, modeling, and reanalysis. *Bull. Amer. Meteor. Soc.,* **80,** 2661–2678.

Jin, F.-F., 1997: An equatorial ocean recharge paradigm for ENSO. Part I: Conceptual model. *J. Atmos. Sci.,* **54,** 811–829.

Kalnay, E., and Coauthors, 1996: The NCEP/NCAR 40-Year Reanalysis Project. *Bull. Amer. Meteor. Soc.,* **77,** 437–471.

Kidson, J. E., 1975: Tropical eigenvector analysis and the Southern Oscillation. *Mon. Wea. Rev.,* **103,** 187–196.

Kistler, R., and Coauthors, 2001: The NCEP–NCAR 50-Year Reanalysis: Monthly means CD-ROM and documentation. *Bull. Amer. Meteor. Soc.,* **82,** 247–267.

Larkin, N. K., and D. E. Harrison, 2002: ENSO warm (El Niño) and cold (La Niña) event life cycles: Ocean surface anomaly patterns, their symmetries, asymmetries, and implications. *J. Climate,* **15,** 1118–1140.

Li, T., 1997: Phase transition of the El Niño–Southern Oscillation: A stationary SST mode. *J. Atmos. Sci.,* **54,** 2872–2887.

Lysne, J., P. Chang, and B. Giese, 1997: Impact of the extratropical Pacific on equatorial variability. *Geophys. Res. Lett.,* **24,** 2589–2592.

McPhaden, M. J., 2003: Tropical Pacific Ocean heat content variations and ENSO persistence barriers. *Geophys. Res. Lett.,* **30,** 1480, doi:10.1029/2003GL016872.

Meinen, C. S., and M. J. McPhaden, 2000: Observations of warm water volume changes in the equatorial Pacific and their relationship to El Niño and La Niña. *J. Climate,* **13,** 3551–3559.

——, and ——, 2001: Interannual variability in warm water volume transports in the equatorial Pacific during 1993–99. *J. Phys. Oceanogr.,* **31,** 1324–1345.

Moore, A. M., and R. Kleeman, 1999: Stochastic forcing of ENSO by the intraseasonal oscillation. *J. Climate,* **12,** 1199–1220.

Perigaud, C. M., and C. Cassou, 2000: Importance of oceanic decadal trends and westerly wind bursts for forecasting El Niño. *Geophys. Res. Lett.,* **27,** 389–392.

Philander, S. G. H., 1985: El Niño and La Niña. *J. Atmos. Sci.,* **42,** 2652–2662.

Pierce, D. W., T. P. Barnett, and M. Latif, 2000: Connections between the Pacific Ocean Tropics and midlatitudes on decadal timescales. *J. Climate,* **13,** 1173–1194.

Rasmusson, E. M., and T. H. Carpenter, 1982: Variations in tropical sea surface temperature and surface wind fields associated with the Southern Oscillation/El Niño. *Mon. Wea. Rev.,* **110,** 354–384.

Reiter, E. R., 1978: Long-term wind variability in the tropical Pacific, its possible causes and effects. *Mon. Wea. Rev.,* **106,** 324–330.

Torrence, C., and P. J. Webster, 1998: The annual cycle of persistence in the El Niño/Southern Oscillation. *Quart. J. Roy. Meteor. Soc.,* **124,** 1985–2004.

Trenberth, K. E., 1976: Spatial and temporal variations of the Southern Oscillation. *Quart. J. Roy. Meteor. Soc.,* **102,** 639–653.

——, and D. J. Shea, 1987: On the evolution of the Southern Oscillation. *Mon. Wea. Rev.,* **115,** 3078–3096.

van Loon, H. L., 1984: The Southern Oscillation. Part III: Associations with the trades and with the trough in the westerlies of the South Pacific Ocean. *Mon. Wea. Rev.,* **112,** 947–954.

——, and D. J. Shea, 1985: The Southern Oscillation. Part IV: The precursors south of 15°S to the extremes of the oscillation. *Mon. Wea. Rev.,* **113,** 2063–2074.

——, and ——, 1987: The Southern Oscillation. Part VI: Anomalies of sea level pressure on the Southern Hemisphere and of the Pacific sea surface temperature during the development of a warm event. *Mon. Wea. Rev.,* **115,** 370–379.

Vimont, D. J., S. Battisti, and A. C. Hirst, 2001: Footprinting: A seasonal connection between the tropics and mid-latitudes. *Geophys. Res. Lett.,* **28,** 3923–3926.

——, J. M. Wallace, and S. Battisti, 2003: The seasonal footprinting mechanism in the Pacific: Implications for ENSO. *J. Climate,* **16,** 2668–2675.

Wang, B., R. Wu, and R. Lukas, 1999: Roles of the western North Pacific wind variation in thermocline adjustment and ENSO phase transition. *J. Meteor. Soc. Japan,* **77,** 1–16.

Wang, C., 2001: A unified oscillator model for the El Niño–Southern Oscillation. *J. Climate,* **14,** 98–115.

Wang, X., F.-F. Jin, and Y. Wang, 2003: A tropical ocean recharge mechanism for climate variability. Part I: Equatorial heat content changes induced by the off-equatorial wind. *J. Climate,* **16,** 3585–3598.

White, W. B., 1995: Design of a global observing system for gyre-scale upper ocean temperature variability. *Progress in Oceanography,* Vol. 36, Pergamon Press, 169–217.